Analysis of the Beaufort-Mackenzie Basin, Canada: burial, thermal and hydrocarbon histories

J. Tang and I. Lerche
Department of Geological Sciences, University of South Carolina, Columbia, SC 29208, USA

Received 14 December 1990; revised 7 September 1991; accepted 9 September 1991

The burial, thermal and hydrocarbon histories of Jurassic–Tertiary sedimentary successions were investigated for three structural zones of the Beaufort-Mackenzie Basin using a one-dimensional comprehensive burial history model. The reconstructed geohistories of seven wells indicate two stages of tectonics in the study area: (1) rifting from the Jurassic to Early Cretaceous in structural Zone I and subsequent extension in structural Zone II; and (2) uplift and erosion after rifting, as well as thermal subsidence. The maximum burial of Jurassic–Cretaceous and Tertiary sediments corresponds to the rifting episode. The Late Eocene to Late Miocene uplift caused at least 1000 – 2000 m of sediment to be removed in the study area. The Late Miocene to Pleistocene thermal subsidence resulted in an accumulation of thick fluvial delta sediments (the Iperk sequence) from the Mackenzie Delta to offshore of the Beaufort Sea. Heating episodes from around 150 to 20 Ma in the Tuktoyaktuk Peninsula province and from around 60 to 10 Ma in the central and western part of the basin are indicated by the inversion of vitrinite reflectance data from seven wells. Comparison of the thermal maturation pattern with oil and gas occurrences in seven of the wells indicates that hydrocarbons in Cretaceous reservoirs may have migrated vertically from the Husky Formation, whereas the hydrocarbons in the Tertiary reservoirs may have undergone extensive lateral migration from offshore, where the Richards sequence source rock has a deeper burial history than onshore.

Keywords: Beaufort-Mackenzie Basin, Canada; burial and thermal histories; hydrocarbon migration

Introduction

Two fundamental approaches to oil and gas exploration have been developed: (1) methods designed to locate hydrocarbons *in situ* from direct measurements ahead of the drill; and (2) methods focusing on the progressive evolution of a sedimentary basin considering the degree of thermal alteration of organic material and the timing of hydrocarbon generation, migration and accumulation, which provide an assessment of hydrocarbon prospectivity. Hydrocarbon occurrences depend on three major factors: (1) the sediment burial history of the basin, which is governed by many factors, including sediment supply, mechanical and chemical compaction, tectonic forces, erosional events, intrusive events, sea level changes, and so on; (2) the structural evolution of the basin; and (3) the thermal evolution of sediments in the basin, which controls the thermal maturation of organic materials, and hydrocarbon generation, migration and accumulation.

In this work, a one-dimensional thermal indicator tomography model (He and Lerche, 1989) has been used to simulate the evolutionary processes of the Beaufort-Mackenzie Basin, including the burial, thermal and hydrocarbon generation histories of Jurassic–Tertiary succession. The specific objectives of this study are: (1) to reconstruct the burial paths of Jurassic–Tertiary strata, the amounts of erosion and basement subsidence, from which we interpret the basin evolution; (2) to determine the thermal maturation levels of Jurassic–Tertiary source rocks; and (3) to investigate possible relationships between the maturity of source rocks and present day oil and gas occurrences. Seven wells have been chosen for this study (*Figure 1*).

Regional setting

Figure 2 shows the geological setting of the Beaufort-Mackenzie Basin, which lies at the junction of three crustal elements (Jones *et al.*, 1980). The basin is bounded to the east by the Eskimo Lakes Fault Zone, to the south-west by the Brooks Range and to the north is the Canada Basin. It is suggested that the development of the Beaufort-Mackenzie Basin is related to Arctic plate tectonics (Young *et al.*, 1976). For details on the distribution of strata and the tectonic evolution of the study area, see Young *et al.* (1976), Dixon *et al.* (1985) and Dietrich *et al.* (1989a).

It is emphasized here that there are two opposing views of the tectonic evolution of the study area. One is that the tectonic evolution of the region began its extension from the Early Jurassic and lasted until the Early Cretaceous, and then a compressional history was dominant from the later Cretaceous to present day

0264–8172/92/050510–17

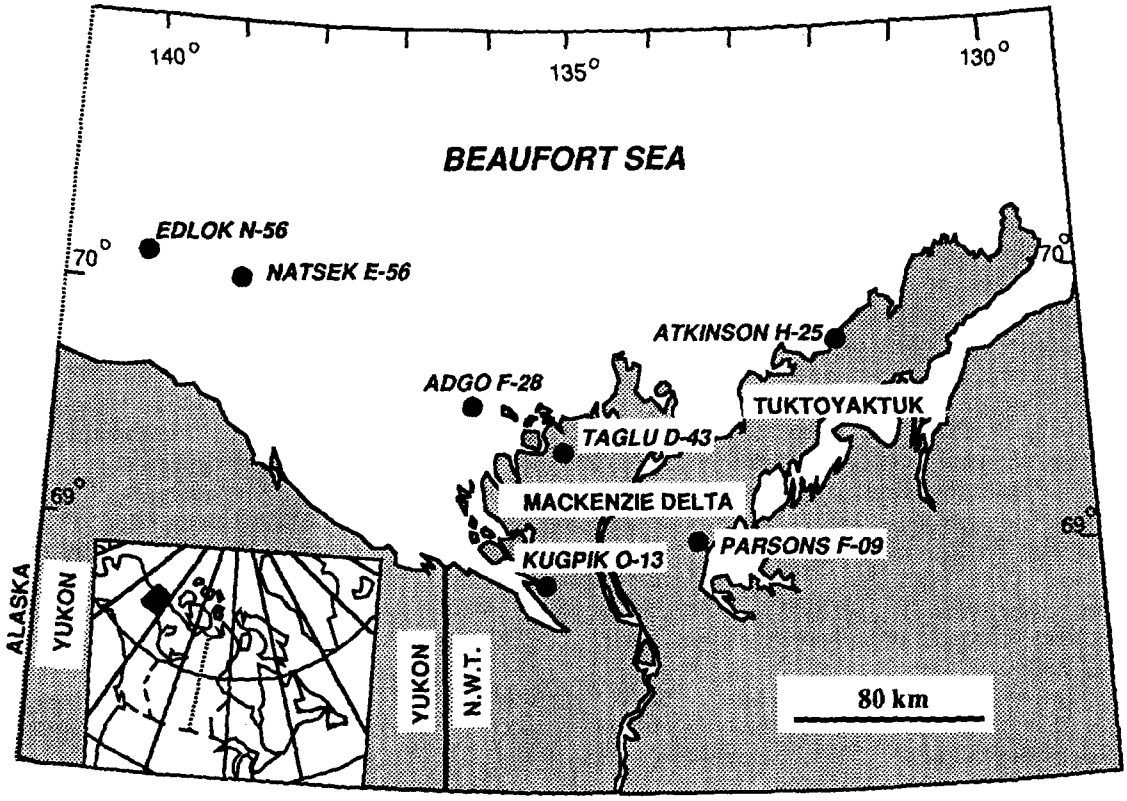

Figure 1 Map of the Beaufort-Mackenzie Basin showing the location of modelled wells (modified from McNeil, 1990)

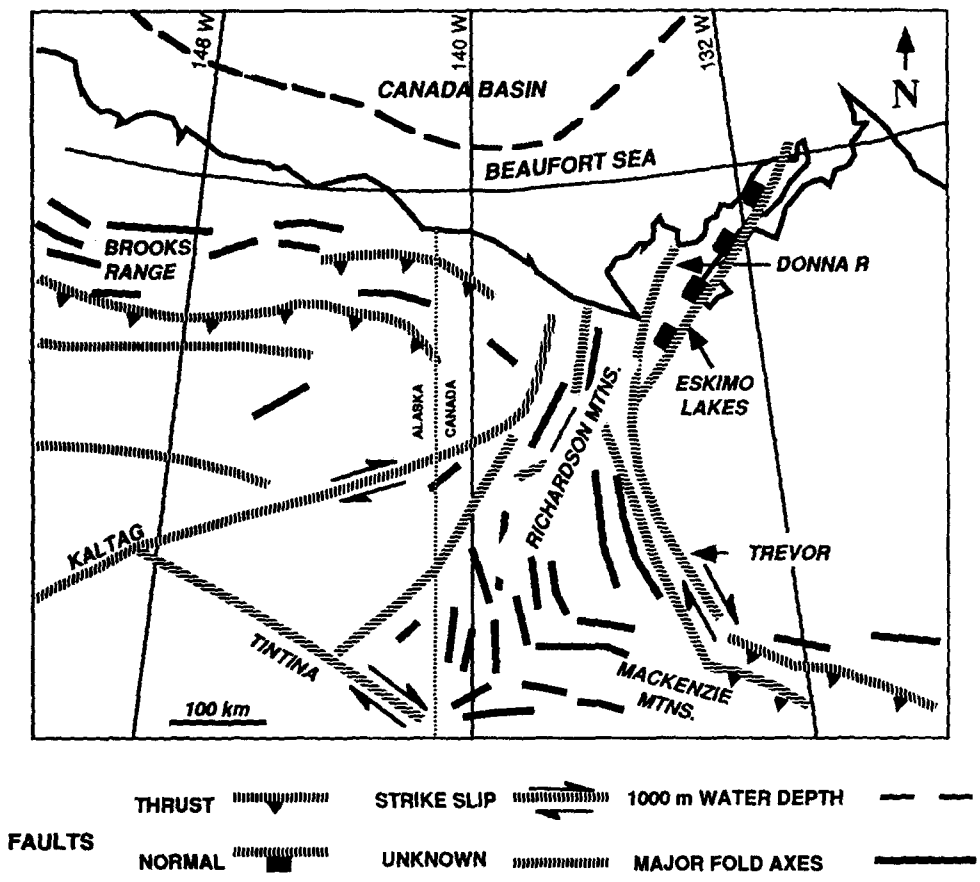

Figure 2 Tectonic map, north-eastern Alaska, northern Yukon Territory and North-west Territories (modified from Jones *et al.*, 1980)

(Dietrich *et al.*, 1989a). The other suggests that the extensional history, lasting to the Middle Miocene, and a later thermal subsidence, resulted in a 14 – 16 km thick sedimentary deposition from the later Cretaceous to present day (Enachescu, 1990).

The stratigraphic framework and nomenclature in the Beaufort-Mackenzie Basin are shown in *Figure 3*. On the basis of lithology, facies distributions and thickness variations of Jurassic to Tertiary strata, Dixon *et al.* (1985) divided the strata into five tectono-stratigraphic assemblages, similar to Young's division of three tectonic-sedimentary phases for Triassic to Tertiary strata in the study area (Young *et al.*, 1976, their Figures 4–16).

In the Jurassic to middle Hauterivian assemblage, sediments were deposited on an epicontinental shelf (Dixon *et al.*, 1985). In the eastern part of the basin, the Husky Formation is considered to be the source unit and the overlying Parsons sandstone is the reservoir unit (Dixon *et al.*, 1985; Cote *et al.*, 1975). In the period from the late Hauterivian to the Albian (the second assemblage), the sediments represent the deposition of low energy shelf and deep water flysch. A major regional unconformity separates Jurassic to middle Hauterivian strata from late Hauterivian to Albian strata. The depositional history is superimposed on an extensional phase of the tectonic development of the Beaufort-Mackenzie Basin.

The Late Cretaceous to Pleistocene strata were divided into three other tectono-stratigraphic assemblages, which were separated by the Late Eocene and Late Miocene unconformities (Dixon *et al.*, 1985). The third assemblage contains six sequences (*Figure 3*). The Boundary Creek and Smoking Hills sequences of the later Cretaceous strata consist of dark grey to black, organic-rich shales. The organic carbon content is in the range 4–12%, which represents deposition in a low energy anoxic marine environment, probably in an outer shelf to slope setting (Dixon *et al.*, 1985). The Fish River sequence is considered to be the first major fluvio-deltaic complex deposited in the Beaufort-Mackenzie Basin (Dixon *et al.*, 1985). The Reindeer and Richards sequences of Early – Middle Palaeocene to Late Eocene strata have been interpreted to be prodelta to delta front to delta plain deposits and a mudstone dominant succession of prodelta to slope deposits, respectively (Dixon *et al.*, 1985). In this assemblage the source rock appears to be the Richards sequences (Snowdon, 1987; 1988; Issler and Snowdon, 1990). The Reindeer and Fish River sequences are the reservoirs in this assemblage (Dixon *et al.*, 1985).

The fourth assemblage consists of the Oligocene Kopanoar and Kugmallit sequences and the Late Oligocene to Late Miocene Mackenzie Bay and Akpak sequences. The former two sequences represent delta plain to slope distal basin plain deposits in which hydrocarbons have been found in the Beaufort Sea (Dixon *et al.*, 1985; Hitchon *et al.*, 1990, Figure 11). The Mackenzie and Akpak sequences represent mud dominant deep water deposits beneath the outer Beaufort Sea shelf and are considered as seals of the Kugmallit reservoir (Dixon *et al.*, 1985; Enachescu, 1990).

The final assemblage consists of the Late Miocene to Pleistocene Iperk sequence, and represents a fluvio-delta depositional complex which rests unconformably on the older strata (Dixon *et al.*, 1985).

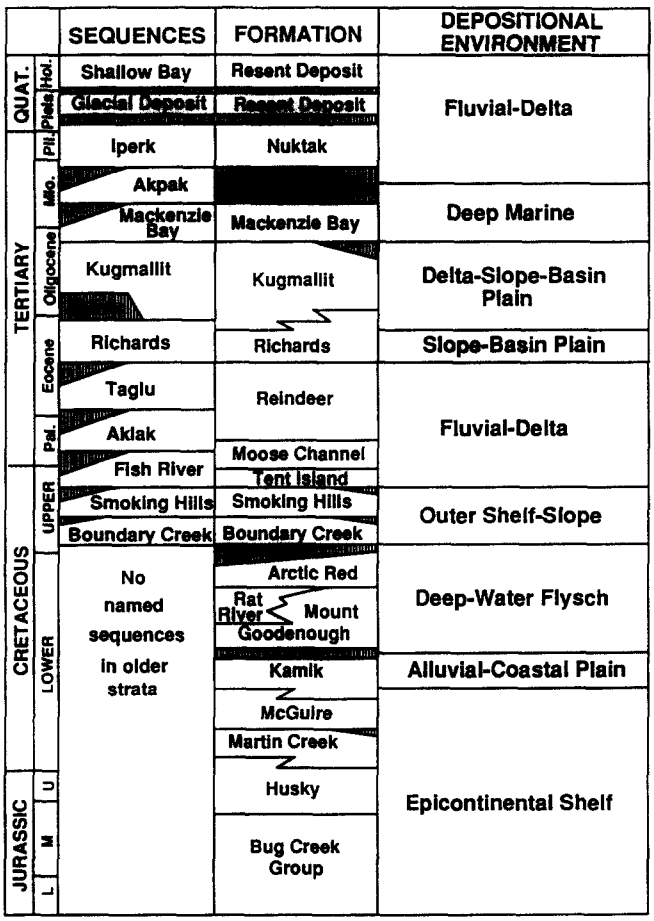

Figure 3 Stratigraphic framework in the Beaufort-Mackenzie Basin (modified from Dixon and Dietrich, 1988)

Structural framework

Based on the distribution, geometry and type of faults in the area and surrounding areas, the Beaufort-Mackenzie Basin can be divided into three structural zones (*Figure 4*; Hawkings *et al.*, 1975; Jones *et al.*, 1980; Enachescu, 1990).

Zone I lies in the south-east, overlying the faulted north-west flank of the Aklavik Arch (*Figure 4*; Jones *et al.*, 1980). Proterozoic and Palaeozoic sedimentary rocks and overlying basal Jurassic and Lower Cretaceous clastics are downfaulted towards, and occasionally away from, the basin. The overlying Upper Cretaceous and Palaeogene sequences are progressively less affected by faulting. Faults include the Eskimo Lakes fault (*Figure 2*; Jones *et al.*, 1980) and the Parsons Lake fault. The Eskimo Lakes fault terminates against, and is interpreted to be offset by, the Donna River fault (*Figure 2*; Jones *et al.*, 1980). Major Columbian tectonic elements, such as the Aklavik Arch and Cache Creek Uplift, do not continue across the Donna River fault and appear to be offset by it. The Parsons Lake gas field and the Atkinson oil discovery lie onshore within Zone I (Jones *et al.*, 1980).

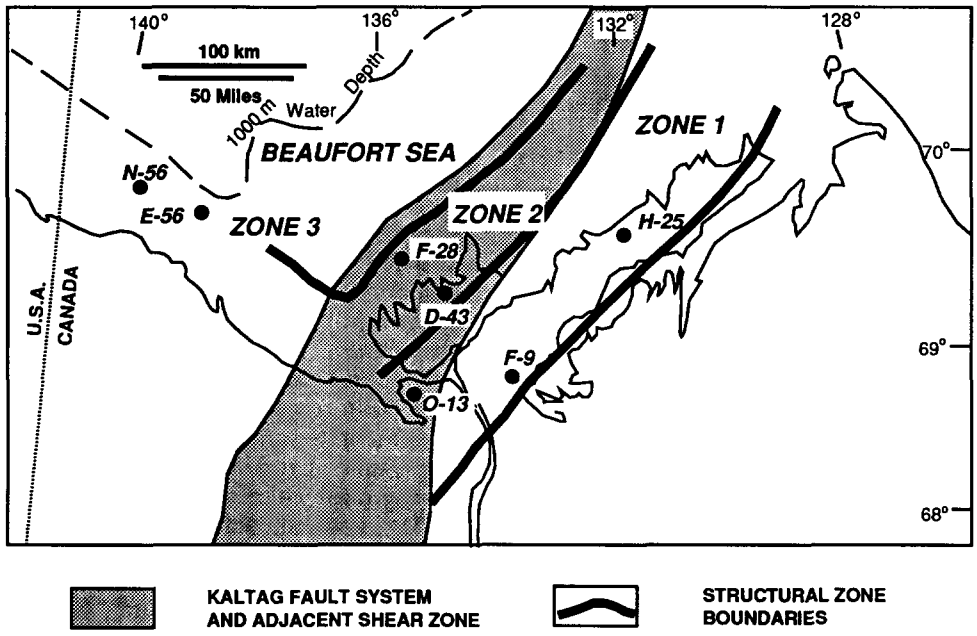

Figure 4 Structural subdivisions, Beaufort-Mackenzie Basin (modified from Jones *et al.*, 1980)

In Zone II, north of the seaward extension of the Donna River fault, Tertiary and possibly Upper Cretaceous clastic sediments are cut by listric growth faults, most of which flatten basinward at depth in thick shale sections. The zone overlies the inferred seaward continuation of the Kaltag fault and associated shear zone. The listric faults are clearly synsedimentary and have no direct connection with deep underlying structures. The Taglu gas field in the Mackenzie Delta lies within Zone II (Jones *et al.*, 1980).

Zone III, to the north-west, including Zone IV of Jones *et al.* (1980), is characterized by shale cored anticlines which are east–west and south-east–north-west trending, in which faults are few and relatively minor (*Figure 4*, Jones *et al.*, 1980).

Source rocks

The Richards sequence, of Tertiary age, and the Smoking Hills and Boundary Creek Formations, of Upper Cretaceous age, as well as the Arctic Red, Mount Goodenough, McGuire and Husky Formations of Jurassic–Lower Cretaceous age, have been considered to be potential source rocks in the study area (Dixon *et al.*, 1985; Issler and Snowdon, 1990).

Total organic carbon (TOC) histograms for the Arctic Red, Mount Goodenough, Husky and McGuire Formations (*Figure 5c*) indicate that all of these formations contain sufficient organic carbon for hydrocarbon generation. The organic matter is dominated by terrestrial (type III) material (Dixon *et al.*, 1985).

For the Upper Cretaceous source rocks, the Smoking Hills and Boundary Creek Formations contain significant amounts of organic carbon (*Figure 5b*) with most of the samples containing more than 3% TOC. The organic matter is composed of a mixture of type III (terrestrial) and type II (marine planktonic) material (Dixon *et al.*, 1985). In structural Zones II and III the source rock is the Tertiary Richards sequence in which the TOC histograms (*Figure 5a*) indicate a moderate, ubiquitous organic content with modal values in the 1–2% range. It is possible that the source quality improves offshore (to the north) where it has not been penetrated, although the Richards sequence has been classified as a poor to marginal source rock where sampled (Issler and Snowdon, 1990). The organic matter in all of the Tertiary delta sediments is totally dominated by higher land plant debris and thus type III kerogen (Dixon *et al.*, 1985).

Basin modelling

So far more than 170 wells have been drilled and 42 oil and gas fields have been discovered in Jurassic and Lower Cretaceous sandstone reservoirs or subunconformity reservoirs along a north-eastern trend of the Tuktoyaktuk Peninsula and in Tertiary strata which are distributed in the area of the Mackenzie River delta and which extend seaward to the north (Enachescu, 1990; Meneley, 1986). The recent oil crisis negatively affected exploration activity in the Canadian north. With the Amauligak J-44 and Kigark J-54 discoveries, however, oil and gas exploration activity is picking up again in the Beaufort-Mackenzie Basin (Enachescu, 1990). To possibly reduce the geological risk in exploration for oil and gas in this area, a method is used here to understand the evolutionary processes of the basin. The method is a one-dimensional thermal indicator tomography program (He and Lerche, 1989; Lerche, 1990), which is applied to seven wells in the Beaufort-Mackenzie Basin. The model is based on a one-dimensional fluid flow–compaction model (Cao, 1985; Cao *et al.*, 1986; Cao and Lerche, 1987). The model consists of three separate components including dynamic models for burial, thermal and hydrocarbon generation histories.

From the burial history model the following results can be obtained: basement subsidence, determination of the thickness of eroded section and the age of an unconformity, and changes in porosity, permeability, fluid flow-rate and pore pressure with time and depth. For the burial history model in this paper, we focused

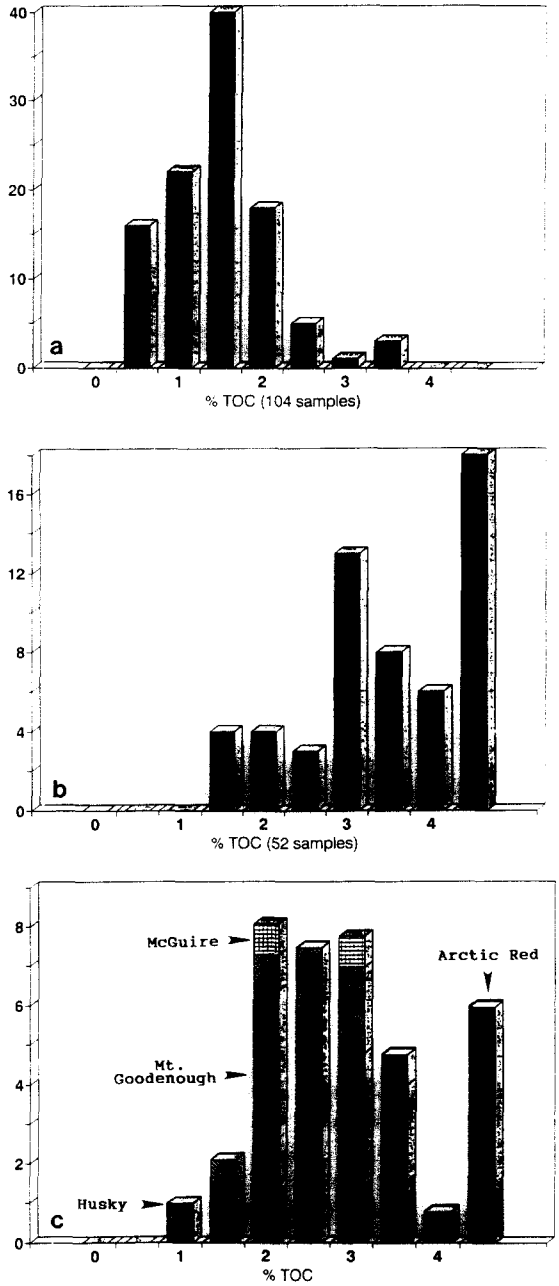

Figure 5 Total organic carbon content. (a) Richards Formation; (b) Smoking Hills and Boundary Creek Formations; and (c) Arctic Red, Mount Goodenough, Husky and McGuire Formations (modified from Snowdon and Brooks, 1985)

on basement subsidence and estimation of the thickness of eroded section. The thermal history model evaluates the change in heat flow through geological time and estimates temperature evolution with time and depth. It is also possible to predict the behaviour of a series of thermal maturity indicators with any given burial history. The hydrocarbon generation model simulates the hydrocarbon generation history from Jurassic to Recent formations of the Beaufort-Mackenzie Basin based on the temperature history, burial history and the kerogen content and type.

Data for basin modelling and procedure

The data used for basin modelling are mainly from Dietrich *et al.* (1989b), Gunther (1976a; 1976b) and Dietrich *et al.* (1989a), which has been chosen as a reference to date the stratigraphy of the seven wells. In structural Zone I, three wells have been chosen: Atkinson H-25, Parsons F-09 and Kugpik 0-13. In Zone II there are two wells, Adgo F-28 and Taglu D-43, and in Zone III two wells, Edlok N-56 and Natsek E-56 (*Figure 4*). The input data for the burial history model are the present day formation thicknesses, the ages of each formation, lithology, water depth at deposition for each formation and present day porosity with depth, if available. The input data used in the thermal history model are vitrinite reflectance and bottom hole temperature or temperature gradient. The surface temperature for each well is set at the average of 2°C for the area. The data for the temperature gradient are from Majorowicz and Dietrich (1989). The Appendix gives vitrinite reflectance data from the seven wells. To run the hydrocarbon generation model, the geochemical character of Jurassic to Tertiary shales (Issler and Snowdon, 1990; Dixon *et al.*, 1985; Snowdon, 1987) indicate type III kerogen for the Tertiary shales, and types II and III kerogen for the Jurassic and Cretaceous shales.

The basic procedure to run the model was as follows. First the calculated thicknesses were obtained, which have to have a best fit with the input thicknesses in the geohistory model. As Cao and Lerche (1987) showed, the simulation of sediment compaction is crucial before running the other two models because the precision of the simulation of sediment compaction affects either directly or indirectly the modelling of thermal and hydrocarbon generation histories. Next, the vitrinite reflectance data from the seven wells were input as the thermal maturation indicator (Appendix). A good fit was obtained between the measured and calculated vitrinite reflectance profiles by adjusting heat flow parameters and by changing the burial paths by adjusting the thicknesses of eroded sediment (He and Lerche, 1989). To obtain a good fit between the measured and calculated reflectance gradients in this area required careful consideration of missing sections at unconformities. If vitrinite reflectance is traced across an unconformity in a measured section, the trend of the vitrinite reflectance profile shows a broad change at the unconformity, where vitrinite reflectance values above the unconformity are markedly less than those below the unconformity. The vitrinite reflectance gradient above the unconformity may be different from the vitrinite reflectance gradient below the unconformity due to a varying thermal history. We determined the heat flow during the unconformity period by using the vitrinite reflectance data above and below. We then varied the amount of sediment removed until the calculated vitrinite reflectance profile matched the measured vitrinite reflectance data on either side of the unconformity (*Figure 6*). Finally, after the uncertainty in each parameter had been minimized [Table 1, Equation (3)], the results of a numerical reconstruction of the burial, thermal and hydrocarbon generation histories were obtained. The errors were estimated by the mean square residual (MSR)

$$\mathrm{MSR} = \frac{1}{N-1}\sum_{i=1}^{N}[VR_c(z_i) - VR_m(z_i)]^2 \qquad (1)$$

where N is the number of measurements of vitrinite reflectance, and VR_c and VR_m are the calculated and

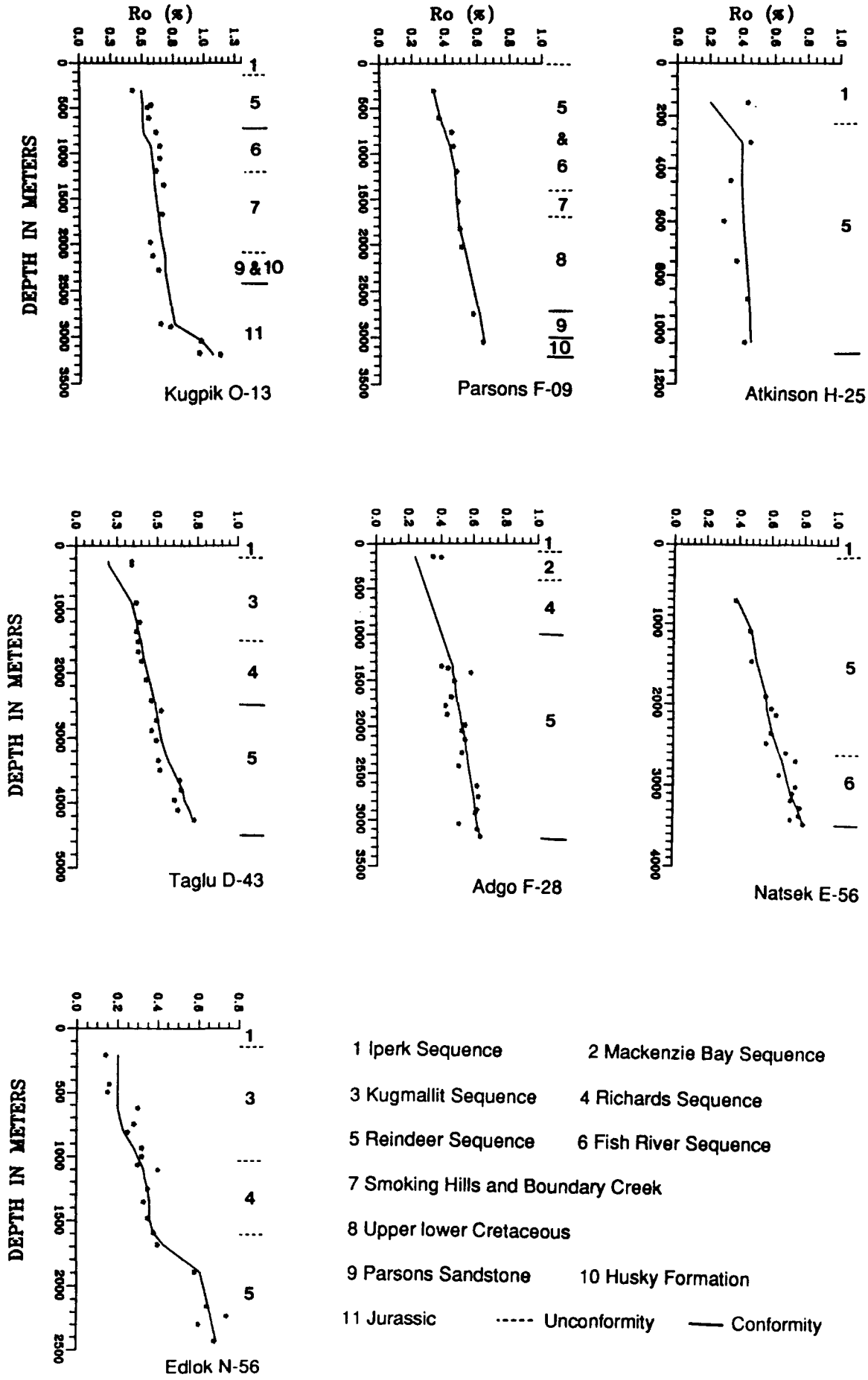

Figure 6 Reflectance versus depth profiles for seven wells in the Beaufort-Mackenzie Basin. Points are measured vitrinite values; solid lines are predicted vitrinite reflectance profiles. The vitrinite reflectance data of Kugpik 0-13, Parsons F-09 and Atkinson H-22 wells are from Gunther (1976a; 1976b) and those of Natsek E-56, Edlok N-56 wells are from Dietrich *et al.* (1989b)

Table 1 Errors between measured and predicted vitrinite reflectance for seven wells

Well:	Atkinson H-25	Parsons F-09	Kugpik 0-13	Taglu D-43	Adgo F-28	Natsek E-56	Edlok N-56
MSR*:	0.17×10^{-1}	0.55×10^{-3}	0.54×10^{-2}	0.34×10^{-2}	0.45×10^{-2}	0.15×10^{-2}	0.24×10^{-2}

*Mean square residual, representing the average degree of mismatch between a series of predicted and measured vitrinite reflectance values. The lower the MSR, the better the fit

measured vitrinite reflectance values at depth z_i, respectively. For example, after the best values of parameters were determined in the burial history modelling, the smallest MSR was 0.5×10^{-3}, which corresponds to the best fit between the observed and predicted vitrinite reflectance values (*Figure 6*), with the best estimate of erosion thickness at 2000 m. If the MSR is doubled relative to its minimum value, the range in thickness of eroded section is about 2000 ± 1000 m at this level of uncertainty. Note that although there are several major unconformities in the Cretaceous–Tertiary strata (*Figure 6*) the 0.33–0.43% of vitrinite reflectance (R_0) recorded for the Tertiary section of the three structural zones near, or at, the present surface (Appendix) indicates that there are two deep erosional events: in the Late Eocene (in structural Zone I) and in the Late Miocene (in structural Zones II and III). Therefore in this study we tried to determine the magnitude of these two erosion events. In addition, the vertical distributions of vitrinite reflectance profiles for the seven wells show that at the upper section the thermal gradient is higher than that at the bottom section. For example, the vitrinite reflectance–depth profile of Parsons F-09 well is characterized by about 0.25%/km in the Tertiary rocks and by about 0.09%/km in the Cretaceous rocks. What causes the variations in thermal gradient except erosional events? We reconstructed the palaeoheat flow variation with time by inversion (Lerche, 1990) to solve this problem.

The following sections give descriptions of the preliminary modelling results for the Beaufort-Mackenzie Basin.

Burial history of the Beaufort-Mackenzie Basin

Figure 7 shows the burial curve patterns at different structural zones. In structural Zone I, the maximum burial of the Jurassic, Cretaceous and Early Palaeocene strata occurred between Eocene and Oligocene times. For example, at well F-09, the Jurassic Husky Formation is indicated to have been buried about 5 km deep. After Eocene uplift and erosion, the Husky Formation is now at a depth of about 3 km. Thus, this uplift and erosion event must have been responsible for the removal of 2000 m of sediments. In structural Zone II, the maximum burial of Tertiary strata occurred during the Late Miocene and then, during Late Miocene (6–5 Ma), about 1000–2000 m of sediment were eroded. Unlike the burial curves in structural Zone II, the maximum depth of burial of Tertiary strata in structural Zone III may not have been reached until about Late Oligocene to Early Miocene times. The amount of erosion is determined to be about 2000 m using the vitrinite reflectance data following the method outlined in He and Lerche (1989).

Figure 8 shows the basement evolution of the Beaufort-Mackenzie Basin with time. The total basement subsidence is divided into two parts, one caused by the weight of sediment and water on the basement and the other caused by tectonic forces, calculated from the isostatic rebound equation (Steckler and Watts, 1978)

$$Y = S\left(\frac{\rho_m - \rho_s}{\rho_m - \rho_w}\right) + Wd - \Delta S_L\left(\frac{\rho_m}{\rho_m - \rho_w}\right) \qquad (2)$$

where Y is the tectonically caused basement subsidence, S is the sediment thickness, Wd is the average water depth at the time of sediment deposition,

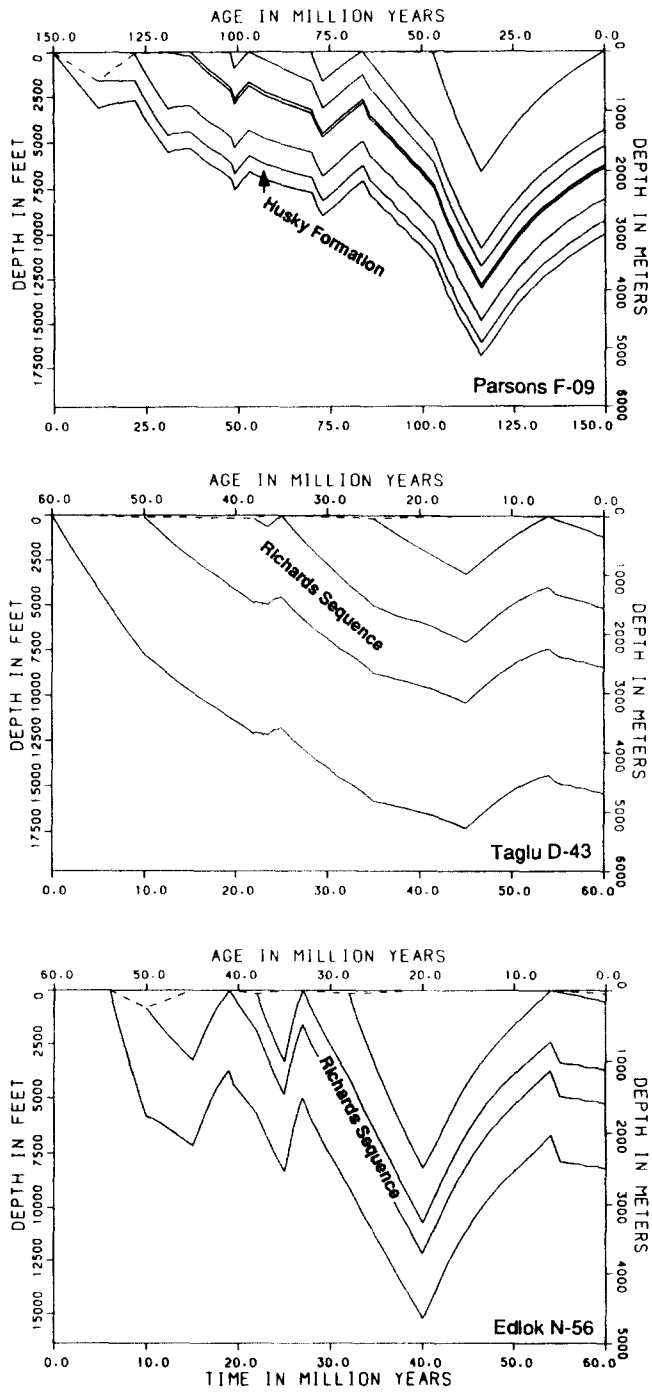

Figure 7 Burial history plots at different structural zones

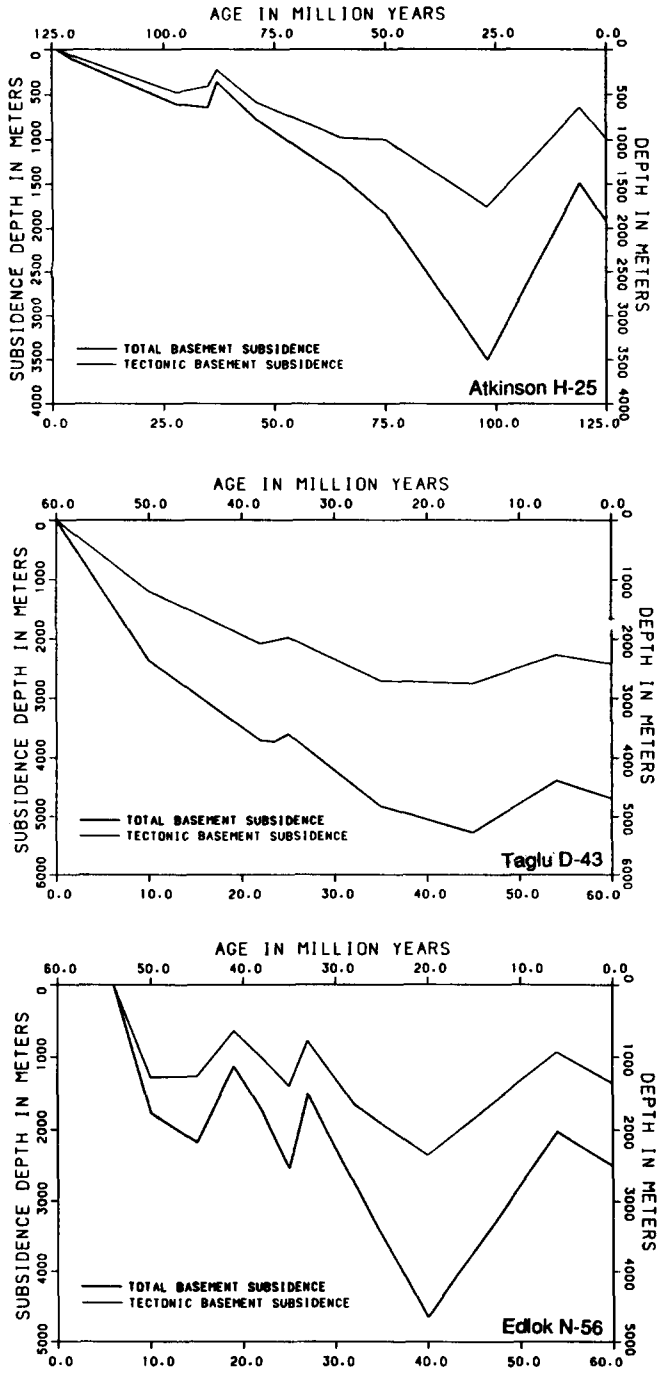

Figure 8 Basement subsidence with time at different structural zones

ΔS_L is the change in elevation of mean sea level, ρ_m is the mantle density, ρ_w is the water density and ρ_s is the average sediment density (the units of Y, S, Wd and ΔS_L are metres and those of ρ_m, ρ_s and ρ_w are kg m^{-3}).

From subsidence patterns in structural Zone I, before and during the Early Cretaceous, the tectonic subsidence did not undergo any sudden change, whereas during the Tertiary the tectonic subsidence obviously increased. For example, the tectonic basement subsided about 500 m up to the early Late Cretaceous and subsided about 1500 m at the end of the Late Oligocene in well Atkinson H-25 (*Figure 8*). Thereafter, there was Late Miocene uplift, followed by thermal subsidence during the deposition of the Iperk sequence. In structural Zone II a sudden change of tectonic subsidence occurred from the Palaeocene to the Oligocene, whereas the tectonic subsidence in structural Zone III underwent a complex phase from the Palaeocene to the present day.

The regional implication is that there were two tectonic stages in the study area. The first is a rifting stage, caused by crustal extension, which continued into the Early Miocene, and which had commenced before the Cretaceous; the second stage is one of uplift and erosion after rifting which may be caused by increased regional palaeoheat flow (in the next section more evidence for this point will be provided). The results of the isostatic rebound model used here to describe the behaviour of the basement with time agree with results obtained using a flexural model (Tang and Lerche, 1992).

Thermal history of the Beaufort-Mackenzie Basin: Palaeoheat flow and palaeotemperature

For reconstruction of the thermal history of the study area, an inverse method called thermal indicator tomography (He and Lerche, 1989) was used to determine the variations in heat flow and temperature with time.

The basement heat flow is described by

$$Q(t) = Q_0\exp[ßt + a_1\sin(\pi t/t_{max}) + a_2\sin(2\pi t/t_{max}) + a_3\sin(3\pi t/t_{max})] \quad (3)$$

where $Q(t)$ is the basement heat flow, Q_0 is the present day heat flow, ß, a_1, a_2 and a_3 are parameters to be determined by minimizing the difference between the predicted and measured vitrinite reflectance with depth, and t_{max} is the age of the deepest sediment for which thermal indicator information is available.

The temperature of each layer at time t and depth $z(t)$ is given by the conventional conduction formula

$$T[t,z(t)] = T_s + Q(t)\int_0^{z(t)} dz/k(z) \quad (4)$$

where T_s is the surface temperature (°C) and $k(z)$ is the sedimentary thermal conductivity ($\approx$1 mcal cm^{-1} s^{-1} °C^{-1}) at depth $z(t)$ (m) described by

$$k(z) = (k_{fl})^{ø(z)}\,(k_s)^{[1-ø(z)]} \quad (5)$$

where k_{fl} is the thermal conductivity of the pore fluid, k_s is the thermal conductivity of the solid rock ($\approx$1 mcal cm^{-1} s^{-1} °C^{-1}), and $ø(z)$ is the porosity at depth z (m) (Lewis and Rose, 1970; Andrews-Speed *et al.*, 1984; Cao and Lerche, 1987).

Plots of measured and predicted vitrinite reflectance (*Figure 6*) show good fits except for well Atkinson H-25 (*Table 1*). The variation of vitrinite reflectance values with depth in well H-25 is abnormal (R_0 = 0.43 at 159 m and 0.42 at 1055 m, *Figure 6*, Appendix). Some of the vitrinite reflectance values are likely to be from reworked kerogen. Therefore the error between the measured and predicted values with depth is relatively larger for this well (*Table 1*) than for the other wells. *Figures 9* and *10* give the heat flow and temperature patterns with time in different structural zones.

In structural Zone I, the reconstructed heat flow histories for the three wells show increasing palaeoheat flow from 150 to 20 Ma and then decreasing palaeoheat

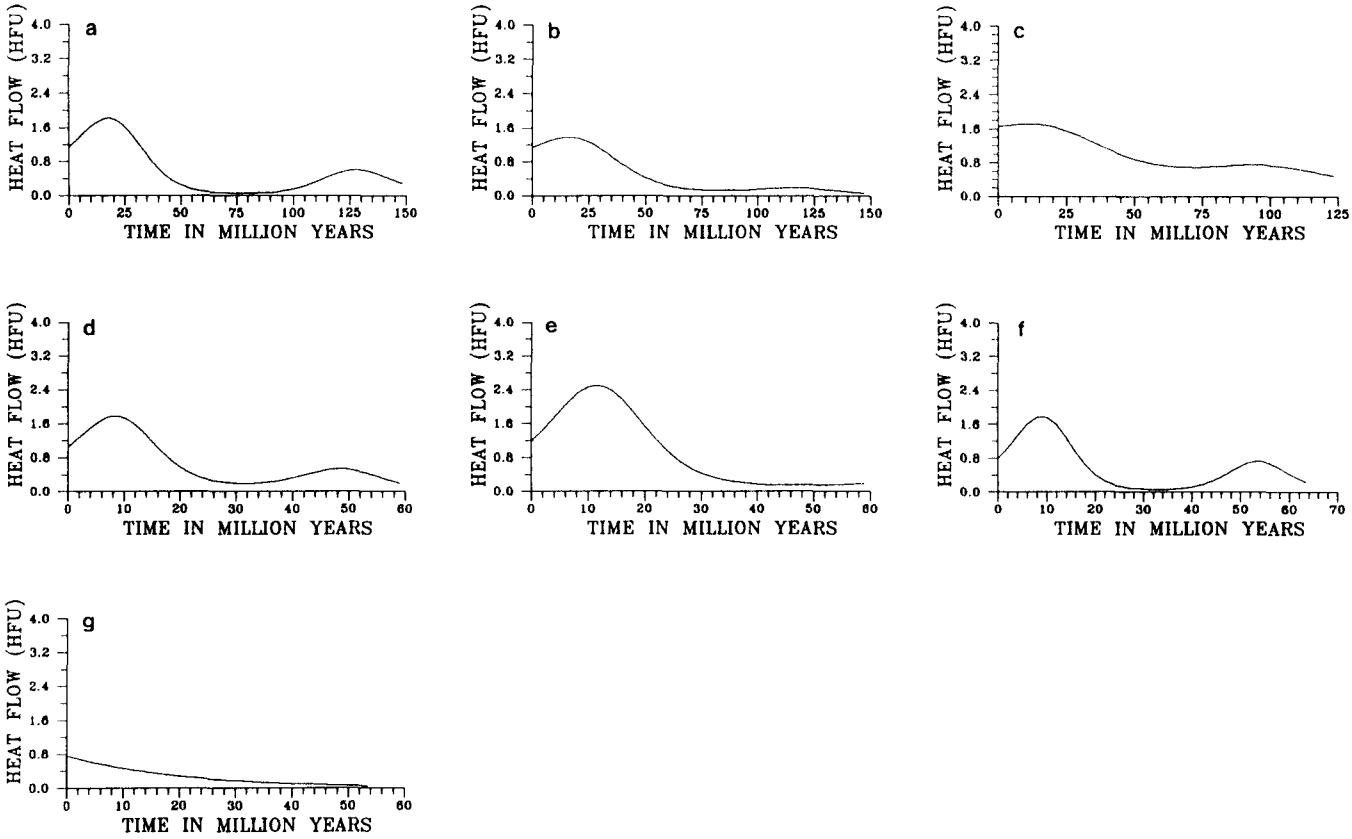

Figure 9 Heat flow evolution with time for the seven wells. (a) Kugpik O-13; (b) Parsons F-09; (c) Atkinson H-25; (d) Taglu D-43; (e) Adgo F-28; (f) Natsek E-56; (g) Edlok N-56

flow from 20 Ma to the present day. In structural Zones II and III the heat flow patterns show increasing palaeoheat flow from 60 to 10 Ma, and then decreasing palaeoheat flow to the present day, except for well N-56 for which the heat flow pattern shows only increasing palaeoheat flow from the past to present day (*Figure 9g*), probably because the vitrinite data do not allow fine enough scale resolution to determine the peak of any heat pulse at around 10 Ma. The temperature variation pattern with time and depth (*Figure 10*) shows a trend similar to that of the heat flow. The temperature anomaly at 20 Ma in structural Zone I and at 10 Ma in structural Zones II and III results from high heat flow during these periods. The cause of the heat flow anomaly can be accounted for as follows. Comparisons between the subsidence patterns (*Figure 8*), thermal history (*Figures 9* and *10*) and burial history (*Figure 7*) suggest that the increase of heat flow from 150 to 20 Ma in structural Zone I may be related to Late Jurassic–Early Cretaceous extension along this region. The geological evidence for the extension of this region is that large marginal faults and a series of subparallel normal faults developed. The increase of heat flow from 60 to 10 Ma in structural Zones II and III may represent a final rifting episode. Associated with the final rifting event is the development of a series of gravity structures (shale diapirism and normal growth faults) in the structural zones. After these two heating stages, the study area began to uplift and erode until 6 Ma. Finally, the thermal subsidence of Late Miocene time allowed deposition of the Iperk sequence. Therefore, it is suggested that the regional structure features and the anomaly patterns of heat flow in this area may result from extensional tectonics. It is argued that seismic data have not supported the suggestion that the rifting was continuous between the Cretaceous and Tertiary (D. G. Roberts, 1991, personal communication). As Roberts pointed out, seismic data across the Aklavik Arch (locations of H-25 and F-09 wells in structural Zone I) do not show evidence of such a prolonged period of extension. The pattern of the basin evolution is one of Late Jurassic–Early Cretaceous extension succeeded by passive subsidence. In contrast, there is evidence of extension in structural Zone II — offshore extension of the Kaltag-Rapid Fault Array (a series of north-trending, high angle faults; Dixon *et al.*, 1985). Connecting this new information provided by Roberts with our modelling results suggests that the Late Jurassic–Early Cretaceous extension caused the development of the Eskimo Lakes Faults (*Figure 2*) and Parsons Lake Fault in the south-eastern margin of the basin. The subsequent extension resulted in the development of shale diapirism and normal growth faults of the Tertiary sediments in the centre of the basin (structural Zone II), whereas the south-eastern margin was subjected to a long lived stage of uplift and erosion or non-deposition from the Late Eocene to Late Miocene (Tang and Lerche, 1992). Also, the heating episode resulted in temperature anomalies which play an important part in hydrocarbon generation and occurrence in the study area.

Thermal maturity of source rocks

Temperature. Iso-temperature lines were obtained by using the best palaeoheat flow variation from the thermal inversion (*Figure 10*). If the 80°C isotherm is considered to be a maturation indicator, the source rocks reached the maturity level at about 4500 m and started about 38 Ma (Late Eocene to Early Oligocene)

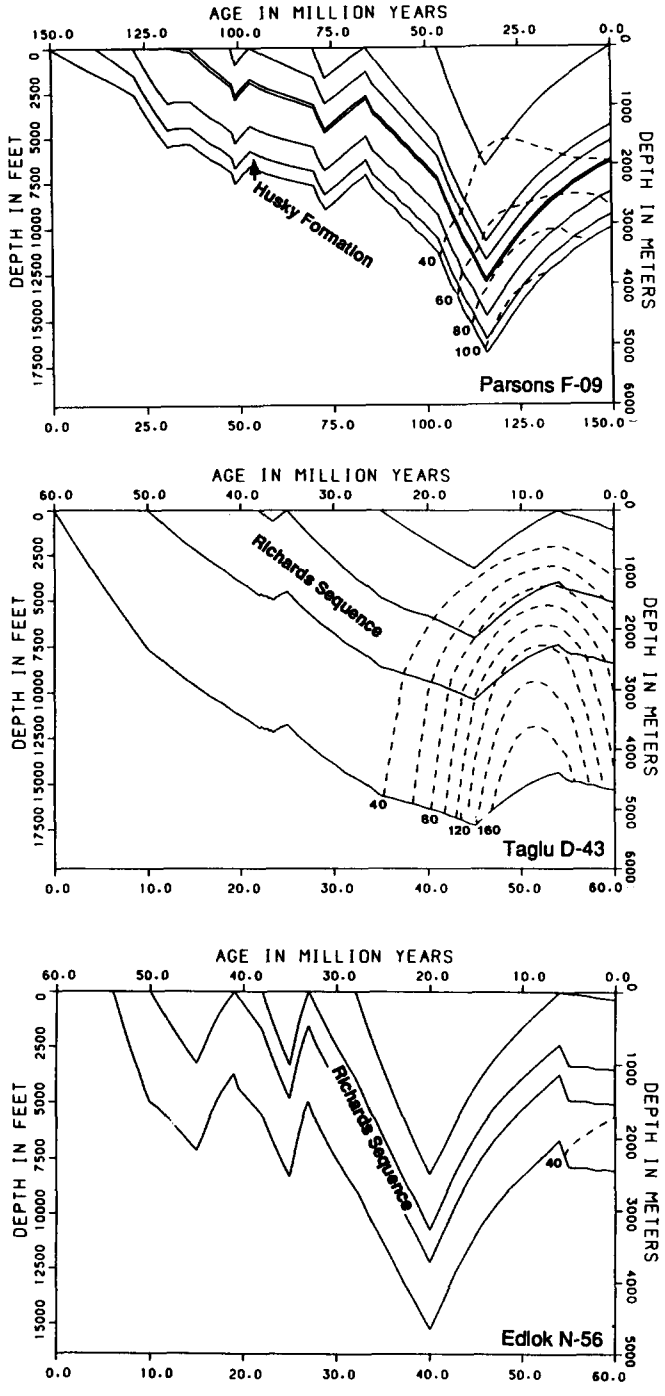

Figure 10 Changes in temperature with time and depth in the study area

in structural Zone I. In structural Zone II the Richards source rock entered the oil window at about 3000 m, and started about the Middle Miocene. At the present day the maturity level is at a depth of 2200 m. The formations in structural Zone III have never reached maturity.

Vitrinite reflectance. Vitrinite reflectance variations with time and depth can be modelled using the equation

$$R[z(t)] = [R_*^{1/2} + \alpha \mathrm{TTI}(t)]^2 \qquad (6)$$

where α is determined from

$$\alpha = \sum_i [R(z_i)^{1/2} - R^{1/2}*] / \sum_i \mathrm{TTI}(t_i) \qquad (7)$$

where $R(z_i)$ is the measured vitrinite reflectance, R_* is the vitrinite reflectance value at the depositional surface (in this instance $R_* = 0.2\%$) and the time – temperature index (TTI) is

$$\mathrm{TTI}(t_i) = \int_0^t \exp[(T - T_c)/T_d]\,dt,\ T > T_c \qquad (8)$$

with the integrand zero in $T < T_c$, where T is the temperature along the burial depth and T_c and T_d are fixed at 295 and 200K, respectively (Lerche, 1988a; 1988b). A vitrinite reflectance of 0.6 has been chosen as marking the onset of the 'oil window'. *Figure 11* shows the evolutionary history of vitrinite reflectance at different structural zones, from which the time when a given source rock enters the 'oil window' is readily

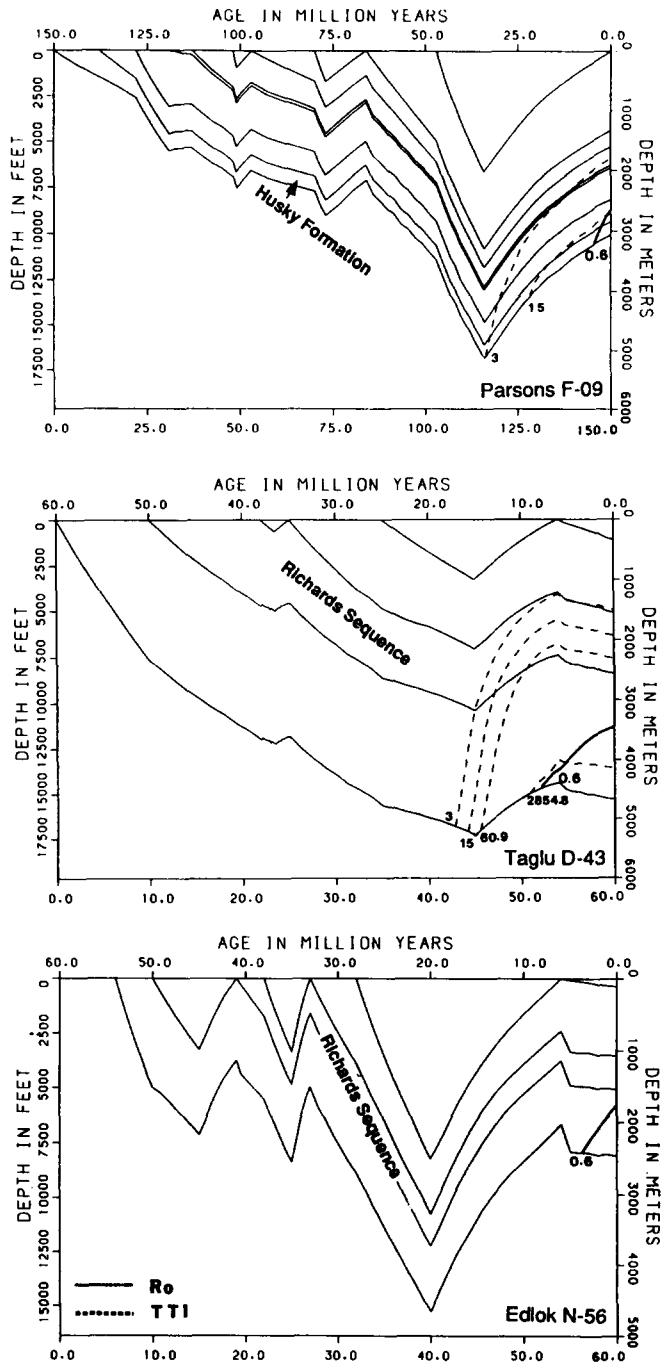

Figure 11 Predicted vitrinite reflectance histories and time-temperature index (TTI) histories in the study area

Table 2 State of maturity of the Upper Jurassic source rocks (the Husky Formation) and the Tertiary source rocks (the Richards sequence) using different thermal indicators at the different structural zones

Structural zone	Depth (m)*			Time of onset (Ma)		
	80°C temperature	R_0 = 0.6%	TTI = 15	80°C temperature	R_0 = 0.6%	TTI = 15
Zone I						
Parsons F-09	4500–3200	3200–2800	4000–2800	38	6	23
Zone II						
Taglu D-43	3000–2200	—†	2800–1900	16	—	12
Zone III						
Edlok N-56	—	—	—	—	—	—

*First value is depth of onset and second value is present day depth of maturity level
†No maturation of source rocks shown

obtained. For example, in structural Zone I, the model predicts that the Upper Jurassic Husky Formation began to enter the oil window in the Late Miocene and at a depth of 3200 m at Parson F-09. At the present day the maturity level is at a depth of 2800 m, which means that the formations deposited earlier than late Early Cretaceous enter the 'oil window'. In structural Zones II and III, the Richards sequence never entered the oil window. At the present day the maturity level is at depths of 3500 and 1800 m, respectively.

Time–temperature index. If a TTI value of 15 (Waples, 1980) is chosen as indicating the onset of the 'oil window', the Husky Formation began to enter the 'oil window' at about 4000 m depth and started in the Late Oligocene in structural Zone I. At the present day the maturity level of the formation is at a depth of 2800 m, the same as the level marked by vitrinite reflectance (*Figure 11*). In structural Zones II and III the depth and timing of maturation (*Figure 11*) based on the TTI thermal indicator are the same as those from the temperature indicator (*Figure 10*).

Table 2 gives the state of maturity of Upper Jurassic and Tertiary source rocks using different thermal indicators in the various structural zones.

Hydrocarbon generation history

To simulate the history of kerogen degradation and hydrocarbon generation in the Beaufort-Mackenzie Basin, the model of Tissot (see, for example, Tissot and Welte, 1978) has been used. *Figures 12* and *13* show the hydrocarbon generation histories for three wells. The simulation results show that oil began to be generated during the Late Eocene–Oligocene in structural Zone I, at a rate of about 50 mg/g kerogen/My. In structural Zone II the Richards sequence began to generate oil in the Early Miocene, at a rate of about 1 mg/g kerogen/My. The source rock in structural Zone III has no hydrocarbon generation history at the lower limit of a rate of about 1 mg/g kerogen/My. The gas generation histories in the study area indicate that the Jurassic Husky Formation has not yet entered the gas window at the location of well F-09 (*Figure 13*). At the locations of wells 0-13 and H-25, the source rocks entered the gas window at the beginning of the Early Oligocene. In structural Zone II, the Richards sequence began to enter the gas window at about 14 Ma. However, the sequence has not entered the gas window at the present

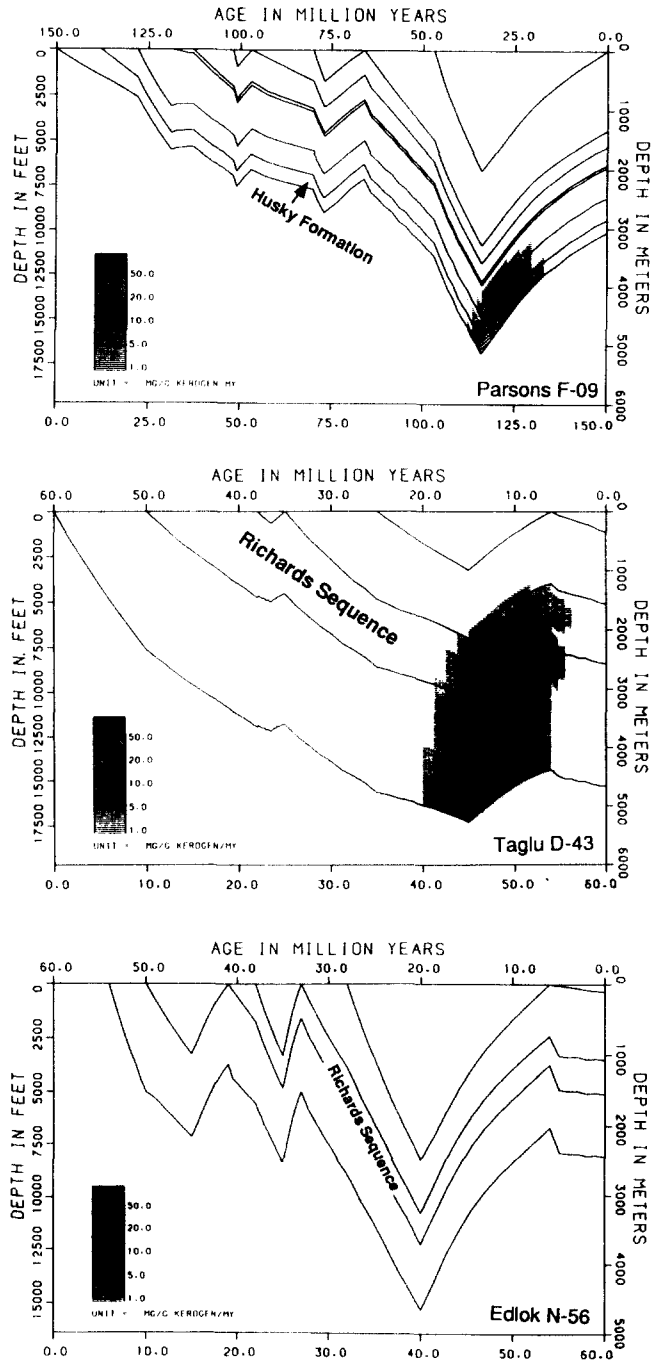

Figure 12 Oil generation histories for three wells

day in structural Zone III (*Figure 13*).

Figure 14 shows the correlation of present day maturity depths of the seven wells from vitrinite reflectance and TTI data. The solid lines represent the bottom boundaries of source rocks with different geological ages; the broken lines represent the predicted vitrinite reflectance of 0.6, which coincides with measured vitrinite reflectance distribution (Appendix) and a TTI of 15. From *Figure 14* the oil window extends from 1100 to 2800 m in structural Zone I, implying that the Jurassic and Cretaceous source rocks (Smoking Hills, Boundary Creek, Arctic Red, Mount Goodenough, Husky and McGuire Formations) have entered the oil window at the locations of Atkinson H-25 and Kugpik 0-13. At the location of Parsons F-09, the Jurassic and Lower Cretaceous source rocks have entered the oil window. In structural Zones II and III, the oil window extends from 1800 to 3500 m, indicating that the Tertiary source rocks (the Richards sequence) are just entering the oil window based on the predicted vitrinite reflectance (R_0 = 0.6). Considering the maturity level (R_0 = 0.6, TTI = 15; *Figure 14*), the TOC of the source rocks (*Figure 5*) and the hydrocarbon generation history (*Figures 12* and *13*) in relation to the observed present day hydrocarbon occurrences, the hydrocarbons of the Tuktoyaktuk Peninsula area (wells 0-13, F-09 and H-25) have Jurassic and Cretaceous sources. In addition to the above factors, considerations of the relationships between reservoir and source rocks suggest that the Tertiary oil and gas (Fish River, Aklak and Taglu sequences, *Figure 3*) are more likely to have Jurassic and Cretaceous source rocks onshore in structural Zone II. Towards the north (offshore), the Richards sequence, as a result of deeper burial, may provide a hydrocarbon source for the overlying reservoir rocks (Kopanoar and Kugmallit sequences). This basic conclusion is supported by observations of hydrocarbon occurrences and by the work of Issler and Snowdon (1990), who point out that the base of the Richards sequence entered the oil window during the Late Oligocene and that peak hydrocarbon generation is presently occurring in the middle of the sequence at the Arluk E-90 and Amauligak J-44 well locations. These observations are consistent with biomarker studies that fingerprint the Richards sequence as the source for offshore Tertiary oils, and the observation that these oils are more mature than their host rocks and therefore have migrated from deeper formations into the shallower reservoirs. Because of the lower maturity level of the Tertiary source rocks in structural Zone III compared with structural Zones I and II, exploration for oil and gas should be focused on the central part of the study area and the Tuktoyaktuk Peninsula.

Uncertainty

The obtained maturity level of source rocks and hydrocarbon generation history of the study area are based on the assumption that the burial history has been determined precisely. Potential errors may arise from uncertainty about the erosion thickness which directly affects the burial path. In other words, uncertainty of erosion thickness results in errors on the maturity level of source rocks and hydrocarbon generation history. In the burial history model the best estimate of erosion thickness for well Parsons F-09 is 2000 m, with the smallest MSR of 0.5×10^{-3}. If the MSR is doubled relative to its minimum value, the range in thickness of eroded section is 2000 ± 1000 m at this level of uncertainty.

Now let us take a look at how much error on the estimate of maturity level this level of uncertainty results in. *Figure 15* shows the profiles of heat flow and temperature versus time for different erosion thicknesses. Large variations in erosion thicknesses cause little change in heat flow (*Figure 15b*), but give a large change in temperature history. The maximum error on temperature is ± 15–20°C/(km of erosion thickness) (*Figure 15a*). The error range on timing maturation of source rocks is about ± 5 My. *Figure 16* shows the profile of vitrinite reflectance and TTI versus depth for different erosion thicknesses from well F-09. We see the same features as on *Figure 15*. The

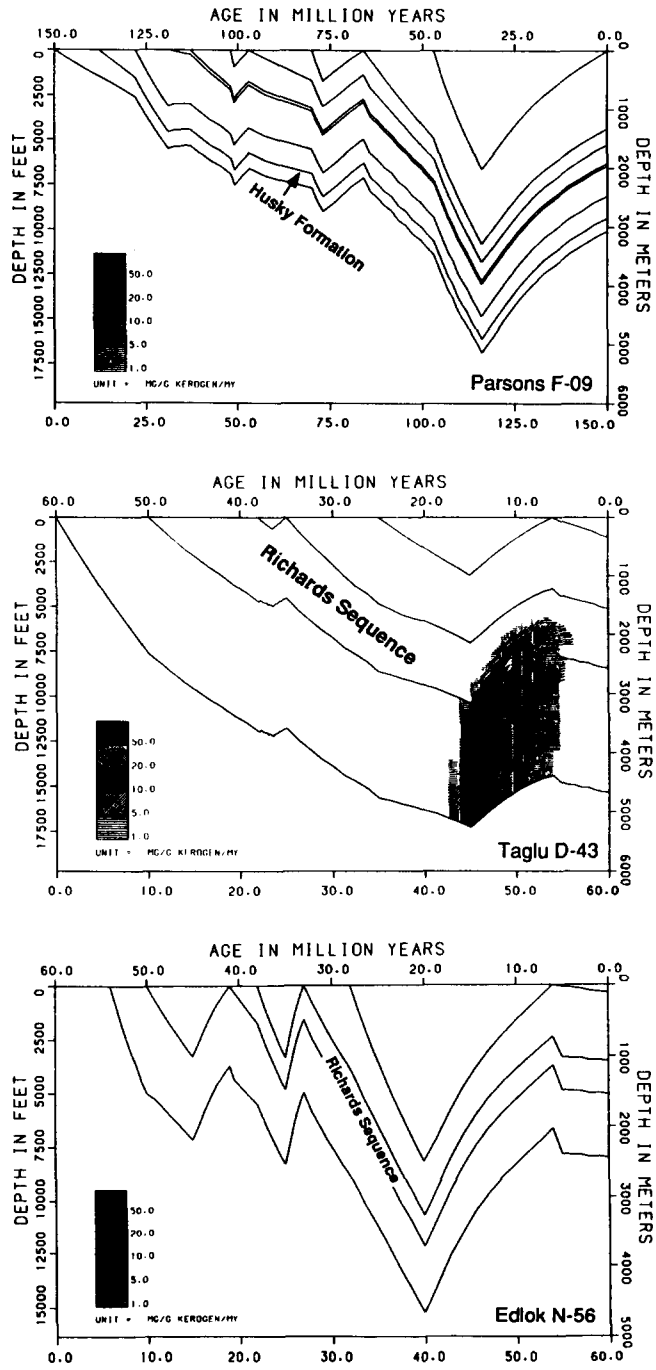

Figure 13 Gas generation histories for three wells

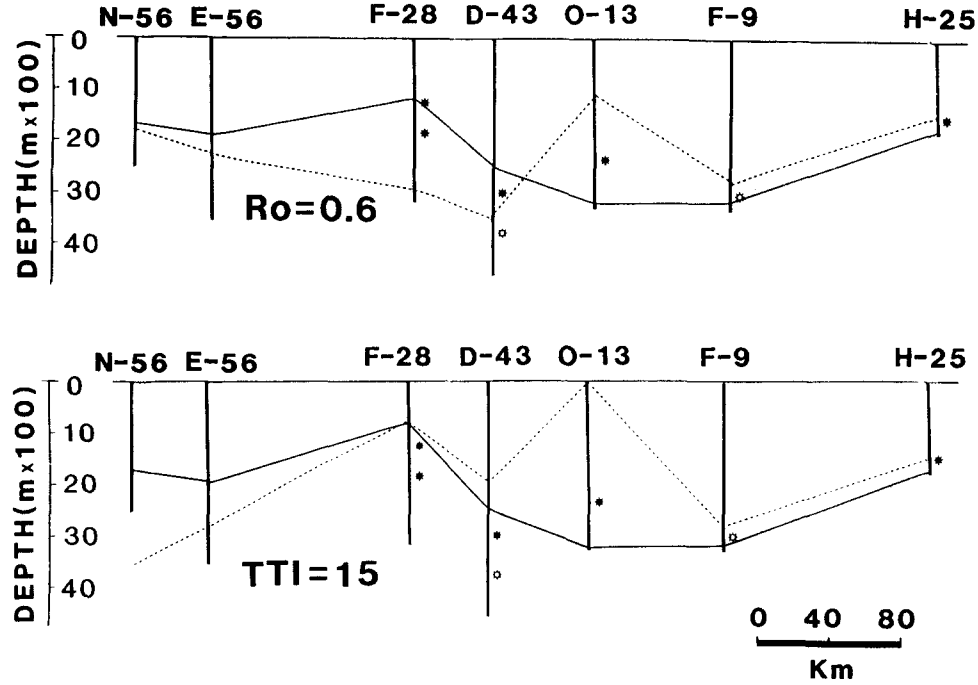

Figure 14 Correlation of present day maturity depth from predicted vitrinite reflectance and TTI. The solid lines represent the bottom boundaries of source rocks (see text) and broken lines represent vitrinite reflectance of 0.6 and a Waples (1980) TTI of 15

variations in erosion thicknesses have more effect on the TTI value than on vitrinite reflectance. This means that the TTI as a thermal indicator is much more sensitive to the burial path. For example, 50% of uncertainty of erosion thickness results in ± 700 m of error range for the determination of maturity depth of source rocks by TTI (*Figure 16b*). At this level of uncertainty vitrinite reflectance only gives an error range of about ± 200 (*Figure 16a*).

The variation of heat flow with time is the key in the reconstruction of thermal history and hydrocarbon generation of source rocks. It is possible that the heat flow variation is linear, a single parameter exponential, or a multi-parameter exponential with time. In this instance heat flow change is described by a multi-parameter exponential model [*Figure 9*, Equation (3)]. We examine here how sensitive the model is to a variable heat flow and how much the uncertainty is to determine the thermal history and hydrocarbon generation with different heat flow patterns. In *Figure 17a*, heat flow patterns 1, 2 and 3 stand for multi-parameter exponential, linear and single-parameter exponential, respectively, for the Parsons well F-09. Pattern 1 was obtained by the best fit procedure with an MSR of 0.6×10^{-3}. For patterns 2 and 3, the MSR is 0.2×10^{-1} and 0.4×10^{-2}, respectively. The error of the MSR of pattern 1 is about 30 times smaller than that of pattern 2 and 10 times smaller than that of pattern 3. *Figure 17b* shows reconstructed palaeotemperature variations with time for the different heat flow profiles. We see that the different heat flows cause significant changes in palaeotemperature. If 80°C is chosen as the onset of 'the oil window', the Husky source rock began to generate hydrocarbons about 80 Ma for pattern 2, whereas pattern 1 gives the time for the Husky source rock to mature and generate hydrocarbons as about 40 Ma. The temperature for pattern 3 (single exponential) was lower than 80°C in the 150 Ma interval.

The uncertainty of heat flow patterns gives the error range on hydrocarbon generation of about 40 My. From these results we see that the model is very sensitive to heat flow patterns which control the

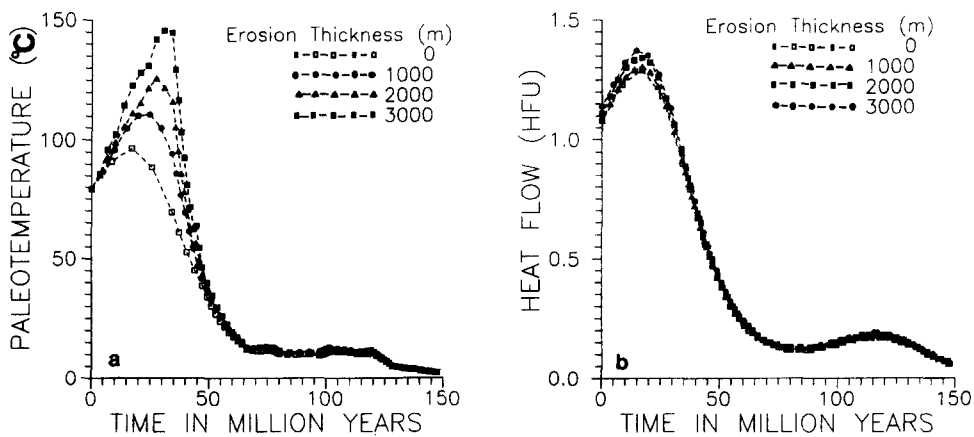

Figure 15 Variations in (a) reconstructed bottom-hole temperature and (b) heat flow with time for different erosion thicknesses

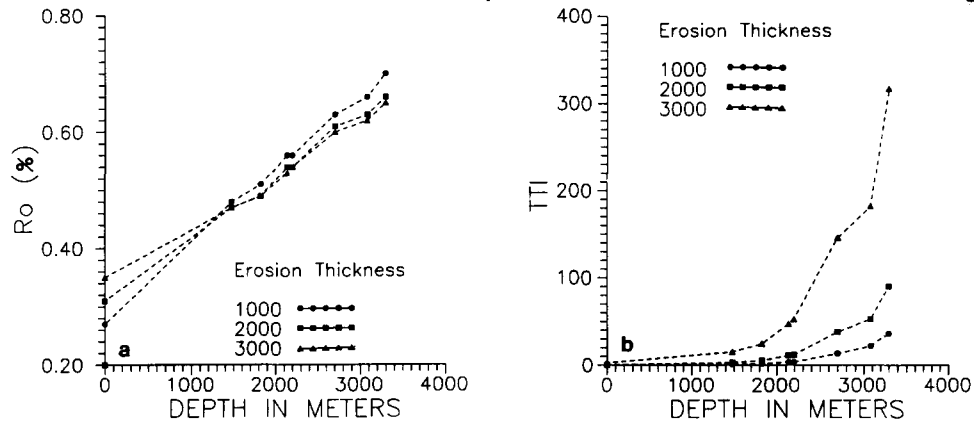

Figure 16 Variations in (a) vitrinite reflectance (R_0) and (b) TTI with depth for different erosion thicknesses

temperature history, and affects the precise determination of maturation and hydrocarbon generation. Therefore it is important to choose different heat flow patterns in models to obtain more representative estimates of the range of uncertainty of thermal evolution and hydrocarbon generation histories.

Figure 18 shows how the TTI and vitrinite reflectance are sensitive to the different heat flow patterns. The TTI is much more sensitive to the pattern behaviour than is vitrinite reflectance. Note that vitrinite is more sensitive to the heat flow pattern in the deeper section than in the shallow burial. Uncertainty in the different heat flow patterns gives an error range on maturity depth of source rocks of about ±300–400 m by vitrinite reflectance as a thermal indicator (*Figure 18b*).

Conclusions

A general picture of the subsidence, thermal and hydrocarbon generation histories of the Beaufort-Mackenzie Basin has been developed using downhole well data and a comprehensive burial history model. The results of this study are now summarized.

The subsidence history model simulates the burial paths of Jurassic to Pleistocene strata in the three structural zones, including erosion thickness and basement behaviour. The maximum burial of Jurassic–Cretaceous and Tertiary sediments is during the Eocene–Oligocene and Late Miocene, respectively. After the deep burial, the Late Eocene uplift and erosion (which lasted until the Late Miocene) caused at least 2000 m of sediment to be removed in structural Zone I. The Late Miocene uplift and erosion event in the central and western parts of the study area resulted in 1000–2000 m of sediment being removed.

Based on interpreted basement behaviour and reconstructed palaeoheat flow patterns and some new information provided by D. G. Roberts (personal communication), two stages of tectonics have been recognized in the study area. The first, a rifting stage, caused the development of the Eskimo Lakes Fault and Parsons Lake Fault in structural Zone I during the Late Jurassic–Early Cretaceous period. The subsequent extension results in the development of a series of gravity structures in structural Zone II. The second, post-rifting uplift and erosion, may have been caused by increased palaeoheat flow, as well as thermal subsidence from the Late Miocene to the present day.

Based on interpretations of vitrinite reflectance data, heating episodes occurred from 150 to 20 Ma in structural Zone I and 60 – 10 Ma in structural Zones II and III. The temperature anomaly is likely to have resulted from the higher heat flow during the Late Oligocene – Late Miocene.

The Richards sequence of Tertiary age and the Husky Formation of Jurassic age have been considered to be major potential source rocks in the study area.

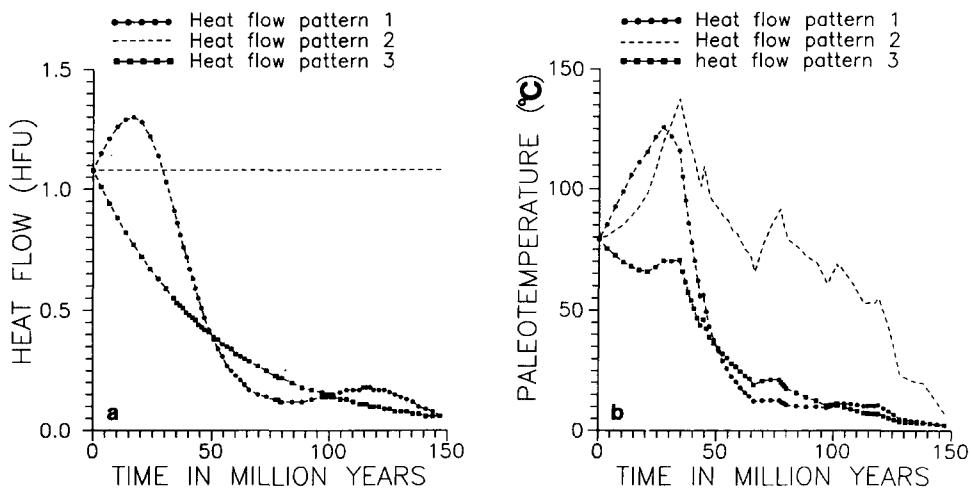

Figure 17 Variations in (a) heat flow and (b) bottom-hole temperature with time for different heat flow patterns (linear, single-parameter exponential and multi-parameter exponential)

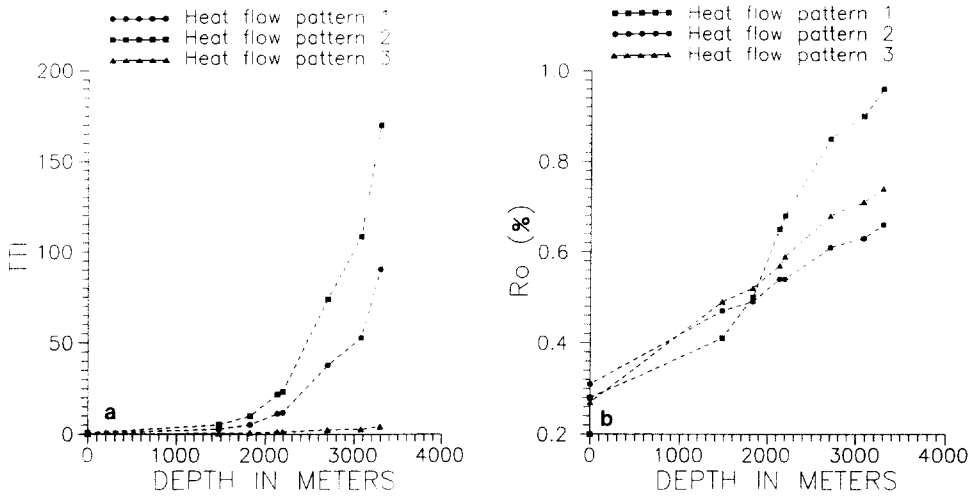

Figure 18 Variations in (a) TTI and (b) R_0 with depth for different heat flow patterns

Peak hydrocarbon generation for the Husky Formation and the Richards sequence in the study area occurred during the Late Eocene to later Oligocene, and mid- to later Miocene, respectively.

The hydrocarbon generation model results suggest that the hydrocarbon potential is higher in the central part (onshore and offshore) and the Tuktoyaktuk Peninsula than in the west part of the study area (structural Zone III). The one-dimensional model, however, assumes that fluid movement was vertical; lateral migration of hydrocarbons is not considered. Lateral migration of oil and gas due to tectonic activity during the Late Miocene may have significantly affected the accumulation or removal of hydrocarbons in the study area.

Uncertainty analysis on erosion thickness and on different heat flow patterns provide assessments of the degree of confidence to attach to the model results. The 50% variation in erosion thickness gives ±5 My of error range on the timing of source rocks entering the 'oil window'. This level of uncertainty yields error ranges of maturity depth of source rocks at the present day as ±700 and ±200 m by the TTI and vitrinite reflectance methods, respectively. The model is very sensitive to heat flow patterns. In this instance the uncertainty of heat flow patterns provides 40 My of error range on the timing of maturation and hydrocarbon generation. The error range of maturity depth of source rocks is ±300–400 m using vitrinite reflectance.

Acknowledgements

The work reported here was supported by the Industrial Associates of the Basin Analysis Group at the University of South Carolina. We thank the Petroleum Geology and Basin Analysis Section, Alberta Geological Survey, Alberta Research Council for their very generous supply of data which enabled this study to be completed. We also thank Brian Hitchon and Stefan Bachu for the critical and insightful comments on an earlier draft of this paper. The manuscript was improved with suggestions and information from Dr D. G. Roberts.

References

Andrews-Speed, C. P., Oxburgh, E. R. and Cooper, B. A. (1984) Temperature and depth-dependent heat flow in West North Sea *Am. Assoc. Petrol. Geol. Bull.* **68**, 1764–1781

Cao, S. (1985) Quantitative dynamic model for basin analysis and its application to the northern North Sea Basin *MS Thesis*, University of South Carolina, Columbia, 94 pp

Cao, S. and Lerche, I. (1987) Geohistory, thermal history and hydrocarbon generation of the northern North Sea Basin *Energy Explor. Exploit.* **5**, 315–355

Cao, S., Glezen, W. H. and Lerche, I. (1986) Fluid flow, hydrocarbon generation and migration: a quantitative model of dynamical evolution in sedimentary basins *Proceedings of the Offshore Technology Conference, Houston, TX, USA, paper no. 5182*, Vol. 2, pp 267–276

Cote, R. P., Lerand, M. M. and Rector, R. J. (1975) Geology of the Lower Cretaceous Parsons Lake Gas Field, Mackenzie Delta, Northwest Territories. In: *Canada's Continental Margins* (Eds C. J. Yorath, E. R. Parker and D. J. Glass), *Can. Soc. Petrol. Geol. Mem. No. 4*, pp 613–632

Dietrich, J. R., Dixon, J., McNeil, D. H. and Snowdon, L. R. (1989a) *Geology, Biostratigraphy and Organic Chemistry*, brief supplementary notes to accompany a one-day short course sponsored by the Canadian Society of Petroleum Geologists, Calgary, 15 June 1989, 18 pp

Dietrich, J. R., Dixon, J., McNeil, D. H., McIntyre, D. J., Snowdon, L. R. and Cameron, A. R. (1989b) The geology, biostratigraphy and organic geochemistry of the Natsek E-56 and Edlok N-56 wells, western Beaufort Sea *Geol. Sur. Can. Pap. 89-1G*, pp 133–157

Dixon, J. and Dietrich, J. R. (1988) The nature of depositional and seismic boundaries in Cretaceous–Tertiary strata of the Beaufort-Mackenzie Basin. In: *Sequences, Stratigraphy, Sedimentology: Surface and Subsurface* (Eds D. P. James and D. A. Leckie), *Can. Soc. Petrol. Geol. Mem. No. 15*, pp 63–72

Dixon, J., Dietrich, J. R., McNeil, D. H., McIntyre, D. J., Snowdon, L. R. and Brooks, P. (1985) Geology, biostratigraphy and organic geochemistry of Jurassic to Pleistocene strata, Beaufort-Mackenzie area, northwest Canada *Course Notes*, Canadian Society of Petroleum Geologists, Calgary, 65 pp

Enachescu, M. E. (1990) Structural setting and validation of direct hydrocarbon indicators for Amauligak Oil Field, Canadian Beaufort Sea *Am. Assoc. Petrol. Geol. Bull.* **74**, 41–59

Gunther, P. R. (1976a) A study employing optical methods to evaluate organic metamorphism and oil-generating potential of sediments in the Mackenzie Delta area *District of Mackenzie Project 740032, Report of Activities, Part C; Geol. Surv. Can. Pap. 76-1C*, pp 143–152

Gunther, P. R. (1976b) Palynomorph color and dispersed coal particle reflectance from three Mackenzie Delta boreholes *Geoscience and Man*, Vol. 15, pp 35–39

Hawkings, T. J. and Hatlelid, W. G. (1975) The regional setting of Taglu Field, in Canada's continental margin. In: *Canada's Continental Margins and Offshore Petroleum Exploration* (Ed. C. J. Yorath), *Can. Soc. Petrol. Geol. Mem. No. 4,* pp 633–647

He, Z. and Lerche, I. (1989) Inversion of multiple thermal indicators: quantitative methods of determining paleoheat flux and geological parameters IV. Case histories using thermal indicator tomography *Math. Geol.* **21,** 523–541

Hitchon, B., Underschultz, J. R., Bachu, S. and Sauveplane, C. M. (1990) Hydrogeology, geopressures and hydrocarbon occurrences, Beaufort-Mackenzie Basin *Bull. Can. Petrol. Geol.* **38,** 215–235

Issler, D. R. and Snowdon, L. R. (1990) Hydrocarbon generation kinetics and thermal modelling, Beaufort-Mackenzie Basin *Bull. Can. Petrol. Geol.* **38,** 1–16

Jones, P. B., Brache, J. and Lentin, J. K. (1980) The geology of the 1977 offshore hydrocarbon discoveries in the Beaufort-Mackenzie Basin, N.W.T. *Bull. Can. Petrol. Geol.* **28,** 81–102

Lerche, I. (1988a) Inversion of multiple thermal indicators: quantitative methods of determining paleoheat flux and geological parameters. I. Theoretical development for paleoheat flux *Math. Geol.* **20,** 1–36

Lerche, I. (1988b) Inversion of multiple thermal indicators: quantitative methods of determining paleoheat flux and geological parameters. II. Theoretical development for chemical, physical and geological parameters *Math. Geol.* **20,** 73–96

Lerche, I. (1990) *Basin Analysis: Quantitative Methods,* Vol. I, Academic Press, San Diego, 559 pp

Lewis, C. R. and Rose, S. C. (1970) A theory relating high temperatures and overpressures *J. Petrol. Technol.* **22,** 11–16

Majorowicz, J. A. and Dietrich, J. R. (1989) Comparison of the geothermal and organic maturation gradients of the central and southwestern Beaufort-Mackenzie Basin, Yukon and Northwest Territories *Geol. Surv. Can. Pap. 89-1G,* pp 63–67

McNeil, D. H. (1990) Stratigraphy and palaeocology of the Eocene Stellarina Assemblage Zone (pyrite diatom steinkerns) in the Beaufort-Mackenzie Basin, arctic Canada *Bull. Can. Petrol. Geol.* **38,** 17–27

Meneley, R. A. (1986) Oil and gas fields in the east coast arctic basins of Canada. In: *Future Petroleum Provinces of the World* (Ed. H. T. Halbouty), *Am. Assoc. Petrol. Geol. Mem. No. 40,* pp 143–176

Snowdon, L. R. (1987) Organic properties and source rock potential of two early Tertiary shales, Beaufort-Mackenzie Basin *Bull. Can. Petrol. Geol.* **35,** 212–232

Snowdon, L. R. (1988) Hydrocarbon migration in Mackenzie Delta sediments *Bull. Can. Petrol. Geol.* **36,** 407–412

Snowdon, L. R. and Brooks, P. (1985) Organic geochemistry. Geology, biostratigraphy and organic geochemistry of Jurassic to Pleistocene strata, Beaufort-Mackenzie area, northwest Canada *Course Notes,* Canadian Society of Petroleum Geologists, Calgary, 65 pp

Steckler, M. S. and Watts, A. B. (1978) Subsidence of the Atlantic-type continental margin off New York *Earth Planet. Sci. Lett.* **41,** 1–13

Tang, J. and Lerche, I. (1992) Tertiary flexural evolution of the Beaufort–Mackenzie Basin, Canada *Mar. Petrol. Geol.* **9,** 245–255

Tissot, B. and Welte, D. H. (1978) *Petroleum Formation and Occurrence,* Springer Verlag, New York, pp 500–521

Waples, D. W. (1980) Time and temperature in petroleum formation: application of Lopatin's method to petroleum exploration *Am. Assoc. Petrol. Geol. Bull.* **64,** 916–926

Young, F. G., Myhr, D. W. and Yorath, C. J. (1976) Geology of the Beaufort-Mackenzie Basin *Geol. Surv. Can. Pap. 76-11,* 63 pp

Appendix

Table A1 Vitrinite reflectance data for seven wells in study area

Well name	Age (sequence/formation)	Depth (m)	Average R_0 (%)
Atkinson H-25 (from Gunther, 1976a)	Iperk sequence	159	0.43
	↑	308	0.45
		454	0.33
		607	0.29
	Reindeer sequence	756	0.37
		896	0.44
	↓	1055	0.42
Parsons F-09 (from Gunther, 1976b)	Reindeer/Fish River sequence	305	0.33
		600	0.36
		761	0.44
		915	0.45
	↓	1200	0.47
	Smoking Hill and Boundary Creek sequence	1525	0.48
		1830	0.49
	Upper Lower Cretaceous	2030	0.50
	Parsons Sandstone	2745	0.57
	Husky Formation	3050	0.63
Kugpik 0-13 (from Gunther 1976a)	↑	311	0.42
		472	0.57
	Reindeer sequence	497	0.54
	↓	613	0.55
	↑	774	0.61
		927	0.55
	Fish river sequence	1064	0.64
		1204	0.61
	↓	1359	0.67
		1679	0.66
	Smoking Hills and Boundary Creek sequence	1993	0.56
		2137	0.58
	Parsons/Husky Unit	2289	0.63
		2868	0.64
	Jurassic	2899	0.72
	↑	3051	0.96
		3182	0.90
	↓	3203	1.12
Adgo F-28 (from Gunther, 1976a)	Iperk sequence	155	0.35
	Mackenzie Bay sequence	165	0.40
	↑	1359	0.40
		1381	0.44
		1430	0.58
	Reindeer sequence	1524	0.48
		1695	0.46
		1789	0.42
		1884	0.43
		1996	0.54
		2057	0.52
		2152	0.54
		2294	0.52
		2435	0.50
		2652	0.61
		2765	0.62
		2938	0.60
		3654	0.50
		3115	0.61
	↓	3200	0.63
Taglu D-43	Iperk sequence	256	0.34
	↑	311	0.34
		613	0.32
		914	0.37
	Kugamallit sequence	1067	0.33
		1219	0.39
	↓	1366	0.37
	↑	1524	0.38
		1679	0.38
	Richards sequence	1823	0.40
		2112	0.43
	↓	2438	0.46
	↑	2594	0.52
		2743	0.49
		2896	0.46
		3048	0.46
	Reindeer sequence	3352	0.50
	↑	3505	0.51
		3661	0.61
		3810	0.64
		3962	0.60
		4115	0.62
	↓	4267	0.72
Edlok N-56 (from Dietrich *et al.*, 1989a)	↑	257	0.14
		481	0.16
		544	0.15
	Kugmallit sequence	670	0.30
		798	0.28
		861	0.25
	↓	981	0.32
	↑	1050	0.32
		1115	0.30
	Richards sequence	1155	0.40
		1307	0.35
	↓	1403	0.33
	↑	1530	0.35
		1642	0.38
	Upper Reindeer sequence	1736	0.40
		1940	0.58
		2200	0.64
		2280	0.74
	↓	2343	0.60
	↑	2470	0.68
Natsek E-56 (from Dietrich *et al.*, 1989a)		756	0.38
	Upper Reindeer sequence	1134	0.47
		1512	0.48
		1951	0.57
	↓	2100	0.60
	↑	2179	0.63
	Lower Reindeer sequence	2401	0.60
		2521	0.57
		2644	0.69
		2744	0.75
	↓	2914	0.65
	↑	3064	0.75
	Fish River sequence	3144	0.73
		3224	0.72
		3314	0.78
		3414	0.77
		3460	0.72
	↓	3520	0.80